Optimal control of axial dispersion tubular reactors with recycle: Addressing state-delay through transport PDEs
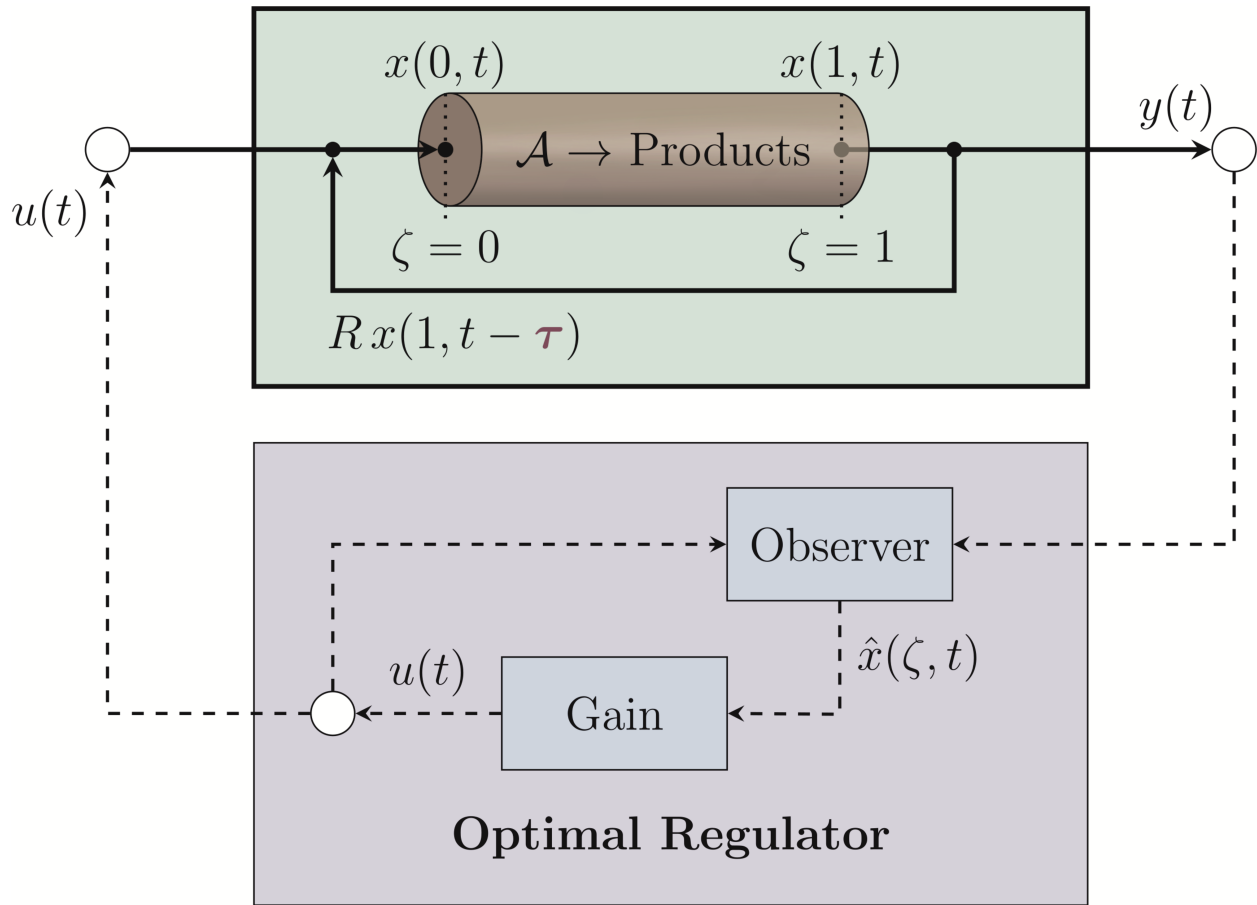
Behrad Moadeli *†   Guilherme Ozorio Cassol*   Stevan Dubljevic *

January 9, 2025

Graphical abstract: The boundary-regulated distributed parameter system of an axial dispersion tubular reactor with delayed recycle is showcased, along with the optimal observer-based control strategy developed using a late-lumping method for its stabilization.

---

*Department of Chemical and Materials Engineering, University of Alberta, Edmonton, Alberta, Canada, T6G 1H9

†Corresponding author. Email: moadeli@ualberta.ca

Abstract

The optimal control of an axial tubular reactor with a recycle stream is addressed as a key type of setting for distributed parameter systems in chemical engineering. The intrinsic time delay from the recycle process, thus far overlooked in relevant literature, is modeled as a transport partial differential equation (PDE), resulting in a system of coupled parabolic and hyperbolic PDEs. Utilizing Danckwerts boundary conditions, the reactor is boundary-controlled with the control input at the inlet. A continuous-time optimal linear quadratic regulator is developed to stabilize the infinite-dimensional system, employing a late lumping approach in order to preserve the properties of the original infinite dimensional system in controller design. The full-state feedback regulator is designed by solving the Operator Riccati Equation (ORE), leveraging the system's Riesz-spectral properties. To address practical limitations of full-state feedback, a Luenberger observer is also proposed, enabling state reconstruction from boundary measurements. Numerical simulations are conducted to evaluate the proposed control strategies. The results demonstrate that the full-state feedback regulator effectively stabilizes the system. A comparison is made between two configurations where different numbers of eigenmodes were selected to design the controller. The observer-based regulator also stabilizes the system successfully using merely output measurements, effectively overcoming the challenge of limited state access.

Keywords: Distributed parameter systems, tubular reactors, recycle, optimal control, state delay

1 INTRODUCTION

Many chemical, petrochemical, and biochemical unit operation processes are modelled as distributed parameter systems (DPS), ranging from tubular reactors, heat exchangers, and separation columns to processes like digesters in the pulp and paper industry and fluid flow in pipeline networks. When these processes are described using first-principle modeling, they result in a class of partial differential equations (PDEs) to effectively capture diffusion, transport, and reaction phenomena, leading to infinite-dimensional state space representations.[ray1981advanced] This characteristic presents significant challenges, making the control and estimation of DPS inherently more complex than finite-dimensional systems. Two primary methods have emerged for addressing DPS control. One is early lumping, which approximates the infinite-dimensional system with a finite-dimensional model.[davison1976robust, francis1977linear] While this method enables the use of standard regulator design techniques, mismatches between the dynamical properties of the original DPS and the approximate lumped parameter model can occur, negatively affecting the performance of the designed regulator.[moghadam2012infinite] The second method is late lumping, which directly tackles the infinite-dimensional system before applying numerical solutions. This approach introduces a challenging yet fertile direction of research, leading to many meaningful contributions that address various aspects of control and estimation of infinite-dimensional systems.

Among notable studies utilizing late lumping method for control of convection-reaction chemical systems resulting in first order hyperbolic PDEs, **christofides1998robust** explored the robust control of quasi-linear first-order hyperbolic PDEs, providing explicit controller synthesis formulas for uncertainty decoupling and attenuation.[christofides1998robust] **krstic2008backstepping** extended boundary feedback stabilization techniques for first-order hyperbolic PDEs using a backstepping method, converting the unstable PDE into a system for finite-time convergence.[krstic2008backstepping] Relevant applications of reaction-convection systems other than tubular reactors have also been addressed within this field, resulting in regulator/observer design strategies for chemical systems governed by first order hyperbolic PDEs. **xu2016state** addressed the state feedback regulator problem for a countercurrent heat exchanger system, utilizing an infinite-dimensional approach to ensure that the controlled output tracks a reference signal.[xu2016state] **xie2021discrete** developed a discrete-time output regulator for gas pipeline networks, emphasizing the transformation of continuous-time models into discrete-time systems while preserving essential continuous-time properties.[xie2021discrete] This work was further extended by **zhang2023tracking**, who proposed a tracking model predictive control and moving horizon estimation design for pipeline systems, addressing the challenges of state and parameter estimation in an infinite-

dimensional chemical system governed by first order hyperbolic PDEs.[zhang2023tracking] For a similar convection-reaction system, **zhang2022dynamic** proposed a model predictive control strategy, incorporating a Luenberger observer to achieve output constrained regulation in a system modeled by nonlinear coupled hyperbolic PDEs.[zhang2022dynamic]

Additionally, diffusion-convection-reaction systems resulting in parabolic PDEs are also addressed in several works. For example, **Christofides2012book** addressed order reduction methods for diffusion-convection-reaction type of reactors.[Christofides2012book] **dubljevic2006predictive2** utilized modal decomposition to capture dominant modes of a DPS to construct a reduced order finite dimensional system, which enables the design of a low dimensional controller for a diffusion-convection-reaction type reactor described by second order parabolic PDEs.[dubljevic2006predictive2] **ozorio2019heat** designed and compared the performance of a full-state and output feedback controller for a diffusion-convection heat exchanger system.[ozorio2019heat] In **khatibi2021model**'s work, an axial dispersion tubular reactor equipped with recycle stream is considered as a second order parabolic DPS, with a predictive controller being utilized to optimally control the reactor. Although the presence of recycle is common in industrial reactor designs, their study has thus far been one of the few contributions in this field addressing a diffusion-convection-reaction system equipped with a recycle stream.[khatibi2021model]

Moreover, continuous-time optimal control design is a well-developed concept for distributed parameter systems, particularly when the system generator is either a self-adjoint operator or can be transformed into one through a proper linear transformation.[morrisbook] However, there are distributed parameter systems that do not possess this property. Instead, the system generator belongs to the class of Riesz-spectral operators. Rather than an orthonormal basis for the function-space, these generators introduce a bi-orthonormal set of eigenfunctions as the basis. Optimal controller design for these systems was initially addressed by **curtainbook**.[curtainbook] Since then, significant work has been done in this field; for instance, continuous-time optimal control design for a cracking catalytic reactor, another convection-reaction system governed by first-order hyperbolic PDEs, has been achieved by solving an operator Riccati equation (ORE).[aksikas2009lq] This work has been further extended to time-varying PDEs of the same class.[aksikas2013optimal] The same approach has been applied to develop a full-state feedback[mohammadi2012lq] and output feedback[aksikas2024spectral] linear quadratic (LQ) optimal regulator for a boundary-controlled convection-reaction system, utilizing the properties of a Riesz-spectral generator for the system.

On top of those dynamic systems that are distributed in space, delay systems are another example of distributed parameter systems.[curtainbook] Although delay is commonly represented in the form of delay differential equations (DDEs), it can also be modeled as a

transport partial differential equation (PDE), which offers advantages in more complex scenarios or when employing alternative norms on infinite-dimensional states. This approach allows for a smoother transition to problems involving more intricate PDE dynamics while maintaining notational consistency.**[krstic2009book]** Input/output delay with relevant applications in chemical engineering has been addressed previously in the field of control theory for DPS. For example, time-delayed boundary observation is considered while addressing an output feedback regulator for a tubular reactor.**[Guilherme2019ACC]** However, the notion of state-delay (as opposed to delayed-inputs or delayed-measurements) seems to be less addressed in this field compared to other relevant fields like signal processing, self-driving cars, or network control theory (NCT). This is probably due to the fact that not many applications in the field of distributed parameter chemical engineering systems can be described by state delays in the first place. **ozorio2019heat**'s work is one of the few instances that addressed a delayed-state distributed parameter chemical engineering system, where they designed a full-state and output feedback regulator for a system of heat exchangers.**[ozorio2019heat]** The notion of state-delay comes from the time it takes for a stream to leave one pass of the heat exchanger and enter the next pass. As stated previously, not much work is published addressing chemical reactors equipped with recycle as distributed parameter systems. Even in **khatibi2021model**'s work, the recycle is assumed to be instantaneous;**[khatibi2021model]** a simplifying assumption that does not resonate well with reality. In fact, taking the time it takes for the recycle stream to re-enter the reactor input can be another instance for the rare concept of a delayed state DPS in the field of chemical engineering. In another attempt, **qi2021output** addressed the challenge of state delay imposed by a recycle stream in a system modeled by interconnected first-order hyperbolic Partial Integro Differential Equations (PIDEs), introducing a transport PDE to account for the in-domain recycle delay.**[qi2021output]** However, the diffusion term was not addressed, leaving a gap in the literature regarding diffusion-convection-reaction systems with a recycle stream imposing state delay.

The present work focuses on the control of an axial tubular reactor equipped with a recycle stream—a configuration common in industrial processes such as catalytic reactors, polymerization units, and biochemical fermenters—but one that is inadequately addressed in the literature. Unlike previous studies that assumed instantaneous recycle, this work incorporates the time delay associated with the recycle stream re-entering the reactor, presenting a rare example of state-delay in the field of chemical engineering DPS. The model comprises a second-order parabolic PDE to capture the diffusion-convection-reaction nature of the reactor, coupled with a first-order hyperbolic PDE to account for the delay. The boundary conditions are chosen as Danckwerts boundary conditions, which are particularly suitable for this type of reactor. The system results in a non-self-adjoint operator. However, by utilizing

the bi-orthogonal theorem, given that the generator is Riesz-spectral, a full-state feedback optimal LQ regulator is developed, followed by an output feedback regulator. The control feedback is derived by solving an operator Riccati equation (ORE) in order to implement a late lumping approach. Actuation and observation are applied at the boundaries, making it a boundary-actuated system involving finite-dimensional dynamics for an infinite-dimensional DPS. These contributions are presented in the following order: In **Section 2**, the system analysis is first addressed by modeling the delay infinite-dimensional system (DPS) and transforming it into a system of coupled PDEs using the delay-transport approach. The system's characteristics are explored by examining the system generator and its eigenvalues, followed by analyzing the adjoint operator and its spectrum, which allows introducing the bi-orthogonal basis for the infinite-dimensional system. Consequently in **Section 3.1**, the design strategy for an optimal full-state regulator is developed by formulating the infinite-time horizon LQ control problem, converting the ORE into matrix Riccati equations (MRE), and calculating the feedback gain. Practical limitations of the full-state feedback mechanism are then addressed in **Section 3.2** by introducing a Luenberger observer for state reconstruction, followed by the design of an output feedback regulator. Finally, numerical simulations are illustrated in **Section 4** to showcase the results of the developed theoretical concepts, demonstrating closed-loop responses of the system equipped with both full-state feedback regulator and output feedback compensator in various settings.
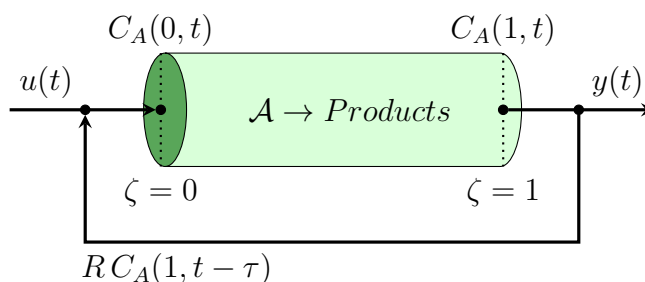
2 OPEN-LOOP SYSTEM

2.1 System model

FIGURE 1: Axial tubular reactor with recycle stream.

The chemical process illustrated in Figure 1 represents an axial dispersion tubular reactor, which incorporates diffusion, convection, and a chemical reaction where reactant A is converted into products.[levenspiel1998chemical] The reactor is equipped with a recycle mechanism,

allowing a fraction of the product stream to re-enter the reactor to ensure the consumption of any unreacted substrate. By applying first-principle modeling through relevant mass balance relations on an infinitesimally small section of the reactor, the dynamics of the reactant concentration can be described by the PDE given in Equation (1), belonging to the class of second order parabolic PDEs commonly used to characterize diffusion-convection-reaction systems[jensen1982bifurcation] in chemical engineering.

$$\dot{C}_A(\zeta, t) = D\partial_{\zeta\zeta}C_A(\zeta, t) - v\partial_\zeta C_A(\zeta, t) + r(C_A) \tag{1}$$

Here, $C_A(\zeta, t)$ denotes the concentration of reactant A along the reactor. The physical parameters D and v correspond to the diffusion coefficient and flow velocity along the reactor, respectively. It is worth noting that the system properties are assumed to be constant against changes in temperature and pressure. The spatial and temporal coordinates of the system are represented by ζ and t, where $\zeta \in [0, 1]$ and $t \in [0, \infty)$. In addition, $r(C_A)$ is the reaction rate by which the reactant is consumed. Considering the reaction term in general can be non-linear, the model is further linearized around its steady-state, followed by replacing the reactant concentration C_A with its deviations from the steady-state concentration $C_{A,ss}$. The result is given in Equation (2).

$$\dot{c}(\zeta, t) = D\partial_{\zeta\zeta}c(\zeta, t) - v\partial_\zeta c(\zeta, t) - k_r c(\zeta, t) \tag{2}$$

where $c(\zeta, t) \equiv C_A(\zeta, t) - C_{A,ss}(\zeta)$ is the deviation from the steady-state concentration and the linearized reaction coefficient is defined as $k_r \equiv \left.\dfrac{\partial r(C_A)}{\partial C_A}\right|_{C_{A,ss}}$ in the vicinity of the steady-state. The system output is assumed to be the deviation of the reactant concentration from the steady-state measured at the reactor outlet, while the control input is set to be equal to the deviation of the reactant concentration from the steady-state, applied at the reactor inlet after being mixed with the delayed state resulting from the recycled portion of the flow occurring τ time units ago. Incorporating input, output, and state delay in addition to the assumption of Danckwerts boundary condition will result in Equation (3) that describe the boundary conditions of the system.

$$\begin{cases} D\partial_\zeta c(0, t) - vc(0, t) = -v\left[Rc(1, t - \tau) + (1 - R)u(t)\right] \\ \partial_\zeta c(1, t) = 0 \\ y(t) = c(1, t) \end{cases} \tag{3}$$

Here, parameters R and τ correspond to the recycle ratio and the residence time along

the recycle stream, respectively. Accounting for deviations from perfect mixing and piston flow and assuming negligible transport lags in connecting lines,[danckwerts1993continuous] the Danckwerts boundary conditions have become an inseparable part of modeling axial tubular reactors in the field of chemical engineering process control and dynamics. While capturing physical significance, Danckwerts boundary conditions maintain generality without unnecessarily simplifying the model as they belong to the general class of Robin boundary conditions.

2.2 PDE representation of the delay term

One effective method for addressing delay in systems is to represent the delay using an alternative transport partial differential equation (PDE). This approach is particularly advantageous when the problem already involves similar forms of PDEs, as is the case in the current study. To specifically address the delay in the system under consideration, the state variable $c(\zeta, t)$ is expanded into a vector of functions $\boldsymbol{x}(\zeta, t) \equiv [x_1(\zeta, t), x_2(\zeta, t)]^T$, where $x_1(\zeta, t)$ is the same as $c(\zeta, t)$, while $x_2(\zeta, t)$ is introduced as a new state variable to account for the concentration along the recycle stream. The delay is thus modeled as a pure transport process, as if the first state $x_1(\zeta, t)$ is being transported from the reactor outlet to the inlet, experiencing a delay of τ time units while in the recycle stream. As a result, Equations 2 and 3 may be re-formulated as follows:

$$\partial_t \begin{bmatrix} x_1(\zeta, t) \\ x_2(\zeta, t) \end{bmatrix} = \begin{bmatrix} D\partial_{\zeta\zeta} - v\partial_\zeta + k_r & 0 \\ 0 & \frac{1}{\tau}\partial_\zeta \end{bmatrix} \begin{bmatrix} x_1(\zeta, t) \\ x_2(\zeta, t) \end{bmatrix} \tag{4}$$

$$\begin{cases} D\partial_\zeta x_1(0, t) - vx_1(0, t) = -v\left[Rx_2(0, t) + (1 - R)u(t)\right] \\ \partial_\zeta x_1(1, t) = 0 \\ x_1(1, t) = x_2(1, t) \\ y(t) = x_1(1, t) \end{cases} \tag{5}$$

With all state variables now expressed explicitly at a specific time instance t—in contrast to the previous representation where states at t were directly involved with states at $(t - \tau)$—the open-loop system can be described in the standard state-space form of an infinite-dimensional linear time-invariant (LTI) system as $\dot{\boldsymbol{x}} = \mathfrak{A}\boldsymbol{x}$. Here, $\mathfrak{A}$ is a linear operator $\mathcal{L}(X)$ acting on a Hilbert space $X : L^2[0, 1] \times L^2[0, 1]$ and $\boldsymbol{x}(\zeta, t)$, as defined previously, is the vector of functions describing the states of the system. The operator $\mathfrak{A}$ and its domain are defined in detail as shown in Equation (6):

$$\mathfrak{A} \equiv \begin{bmatrix} D\partial_{\zeta\zeta} - v\partial_\zeta + k_r & 0 \\ 0 & \frac{1}{\tau}\partial_\zeta \end{bmatrix}$$

$$\mathcal{D}(\mathfrak{A}) = \Big\{ \boldsymbol{x} = [x_1, x_2]^T \in X : \boldsymbol{x}(\zeta), \partial_\zeta \boldsymbol{x}(\zeta), \partial_{\zeta\zeta}\boldsymbol{x}(\zeta) \quad \text{a.c.},$$

$$D\partial_\zeta x_1(0) - vx_1(0) = -v\left[Rx_2(0) + (1-R)u\right],$$

$$\partial_\zeta x_1(1) = 0, x_1(1) = x_2(1) \Big\}$$

(6)

2.3 Adjoint operator

The adjoint operator $\mathfrak{A}^*$ plays a critical role in analyzing the spectral properties of the system. It is obtained in Equation (7):

$$\langle \mathfrak{A}\boldsymbol{\phi}, \boldsymbol{\psi} \rangle = \langle \boldsymbol{\phi}, \mathfrak{A}^*\boldsymbol{\psi} \rangle \Rightarrow$$

$$\mathfrak{A}^* = \begin{bmatrix} D\partial_{\zeta\zeta} + v\partial_\zeta + k_r & 0 \\ 0 & -\frac{1}{\tau}\partial_\zeta \end{bmatrix}$$

$$\mathcal{D}(\mathfrak{A}^*) = \Big\{ \boldsymbol{y} = [y_1, y_2]^T \in Y : \boldsymbol{y}(\zeta), \partial_\zeta \boldsymbol{y}(\zeta), \partial_{\zeta\zeta}\boldsymbol{y}(\zeta) \quad \text{a.c.},$$

$$D\partial_\zeta y_1(1) + vy_1(1) = \frac{1}{\tau}y_2(1)$$

$$Rvy_1(0) = \frac{1}{\tau}y_2(0)$$

$$\partial_\zeta y_1(0) = 0 \Big\}$$

(7)

where $\boldsymbol{\phi_i}(\zeta) = [\phi_{i,1}(\zeta), \phi_{i,2}(\zeta)]^T$ and $\boldsymbol{\psi_i}(\zeta) = [\psi_{i,1}(\zeta), \psi_{i,2}(\zeta)]^T$ are the eigenfunction of $\mathfrak{A}$ and $\mathfrak{A}^*$, respectively. Given that $\mathfrak{A}$ is not self-adjoint (i.e., $\mathfrak{A} \neq \mathfrak{A}^*$), their combined eigenmodes may still form a bi-orthonormal basis, typical of a Riesz-spectral operator.**curtainbook** Therefore their spectral properties must be determined by solving their characteristic equations.

2.4 Eigenvalue problem

The eigenvalue problem for $\mathfrak{A}$ is formulated as:

$$\mathfrak{A}\boldsymbol{\phi_i}(\zeta) = \lambda_i \boldsymbol{\phi_i}(\zeta) \tag{8}$$

where $\lambda_i \in \mathbb{C}$ is the ith eigenvalue. To obtain the characteristic equation, the system of PDEs shall be reduced to the ODE system in Equation (9) $\forall i \geq 0$:

$$\partial_\zeta \begin{bmatrix} \phi_1 \\ \partial_\zeta \phi_1 \\ \phi_2 \end{bmatrix} = \begin{bmatrix} 0 & 1 & 0 \\ \frac{\lambda - k_r}{D} & \frac{v}{D} & 0 \\ 0 & 0 & \tau\lambda \end{bmatrix} \begin{bmatrix} \phi_1 \\ \partial_\zeta \phi_1 \\ \phi_2 \end{bmatrix} \tag{9}$$

which is in the form of $\tilde{\boldsymbol{\phi}}_\zeta = \tilde{\mathfrak{A}}\tilde{\boldsymbol{\phi}}$, with the solution stated in Equation (10):

$$\begin{bmatrix} \phi_1 \\ \partial_\zeta \phi_1 \\ \phi_2 \end{bmatrix}_{\zeta=1} = \begin{bmatrix} \Lambda_{1,1} & \Lambda_{1,2} & \Lambda_{1,3} \\ \Lambda_{2,1} & \Lambda_{2,2} & \Lambda_{2,3} \\ \Lambda_{3,1} & \Lambda_{3,2} & \Lambda_{3,3} \end{bmatrix} \begin{bmatrix} \phi_1 \\ \partial_\zeta \phi_1 \\ \phi_2 \end{bmatrix}_{\zeta=0} \tag{10}$$

where the 3×3 matrix $\Lambda_{(m,n)}$ is defined as $\Lambda \equiv e^{\tilde{\mathfrak{A}}(\zeta - 0)}\Big|_{\zeta=1}$. By applying the boundary conditions to Equation (10), the algebraic system of equations in Equation (11) is obtained:

$$\begin{bmatrix} -v & D & Rv \\ \Lambda_{2,1} & \Lambda_{2,2} & \Lambda_{2,3} \\ (\Lambda_{1,1} - \Lambda_{3,1}) & (\Lambda_{1,2} - \Lambda_{3,2}) & (\Lambda_{1,3} - \Lambda_{3,3}) \end{bmatrix} \begin{bmatrix} \phi_1 \\ \partial_\zeta \phi_1 \\ \phi_2 \end{bmatrix}_{\zeta=0} = \tilde{\Lambda}\,\tilde{\boldsymbol{\phi}}\Big|_{\zeta=0} = 0 \tag{11}$$

where $\tilde{\Lambda}$ is defined as the square matrix shown in Equation (11). Equation (11) suggests that the matrix $\tilde{\Lambda}$ must be rank-deficient for appropriate values of λ_i. Attempts to analytically solve the characteristic equation $det(\tilde{\Lambda}) = 0$ has failed; therefore, it is solved numerically using the parameters in Table 1. The resulting eigenvalue distribution is depicted in Figure 2 in the complex plane.

Following the same procedure for $\mathfrak{A}^*$ shows that the eigenvalues of $\mathfrak{A}$ match the ones of its adjoint, confirming that $\mathfrak{A}$ and $\mathfrak{A}^*$ form a bi-orthogonal basis according to Equation (12):

$$\langle \mathfrak{A}\boldsymbol{\phi_i}, \boldsymbol{\psi_j} \rangle = \langle \lambda_i \boldsymbol{\phi_i}, \boldsymbol{\psi_j} \rangle = \lambda_i \langle \boldsymbol{\phi_i}, \boldsymbol{\psi_j} \rangle$$
$$\text{L.H.S.} = \langle \boldsymbol{\phi_i}, \mathfrak{A}^* \boldsymbol{\psi_j} \rangle = \langle \boldsymbol{\phi_i}, \lambda_j^* \boldsymbol{\psi_j} \rangle = \overline{\lambda_j^*} \langle \boldsymbol{\phi_i}, \boldsymbol{\psi_j} \rangle \tag{12}$$
$$\lambda_i = \overline{\lambda_i^*} \Rightarrow \langle \boldsymbol{\phi_i}, \boldsymbol{\psi_j} \rangle = \delta_{ij}$$

The eigenfunctions $\{\boldsymbol{\phi_i}(\zeta), \boldsymbol{\psi_i}(\zeta)\}$ (for $\mathfrak{A}$ and $\mathfrak{A}^*$, respectively) may be obtained following the calculation of eigenvalues. The first 3 eigenfunctions are plotted in Figure 3.
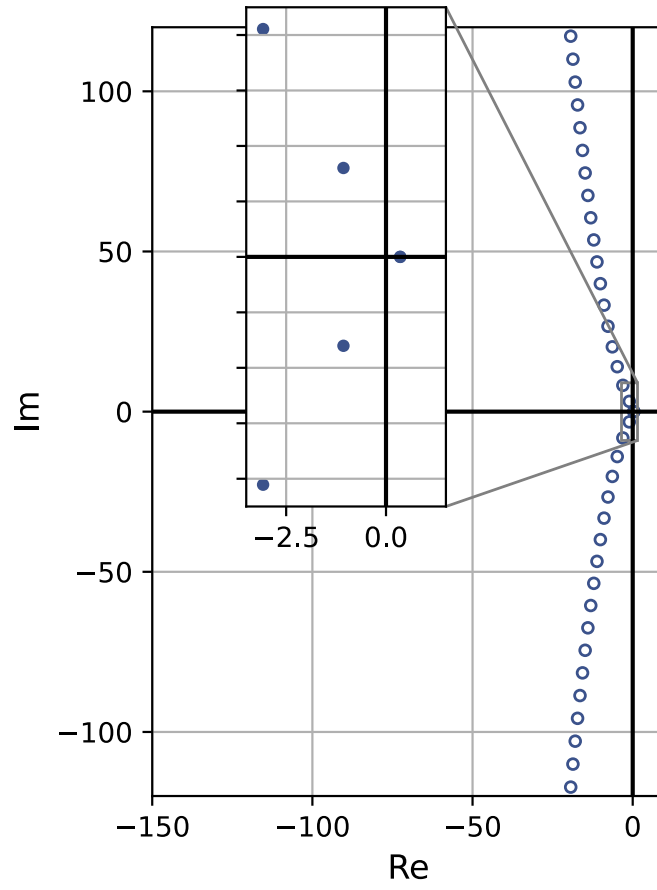
FIGURE 2: Eigenvalues of operator $\mathfrak{A}$ obtained by solving Equation (11).
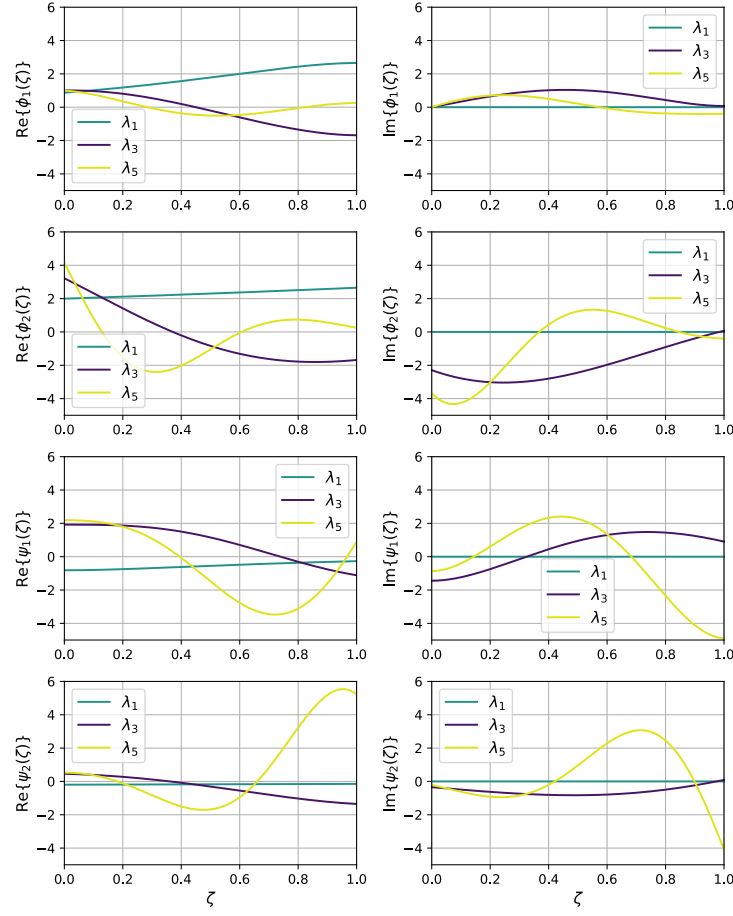
FIGURE 3: First few eigenmodes of $\mathfrak{A}$ and $\mathfrak{A}^*$.

Table 1: Physical Parameters for the System

Parameter	Symbol	Value	Unit
Diffusivity	D	2×10^{-5}	m^2/s
Velocity	v	0.01	m/s
Reaction Constant	k_r	-1.5	s^{-1}
Recycle Residence Time	τ	80	s
Recycle Ratio	R	0.3	$-$

The parameters of the system are carefully chosen to highlight all its key characteristics simultaneously—namely, significant diffusion, convection, and reaction occurring within the reactor—while also ensuring that the delay term and recycle ratio have a pronounced effect on system dynamics. Additionally, the parameters are deliberately selected to introduce instability into the system, emphasizing the proposed control strategy's ability to stabilize an inherently unstable system. While no isothermal reactor can truly exhibit exponential instability due to the finite availability of reactants, such systems can still become unstable

near the steady state. In this context, deviations from the steady state may cause the system to transition toward a different steady state, thereby altering the underlying dynamics and invalidating the original model used for system design and control optimization.

It has been observed that for the linearized system to have an unstable steady state, the reaction coefficient, k_r, must be negative. Although rare, this scenario can arise in certain reaction mechanisms where the reaction rate decreases as the reactant concentration increases, such as autocatalytic reactions, enzyme-catalyzed reactions, or reactions involving inhibitory effects. This instability can be qualitatively understood as follows: a negative reaction coefficient causes a decline in the reaction rate as the reactant accumulates, leading to further reactant accumulation and thus, driving the system away from its steady state. Quantitative confirmation of this behavior can be achieved through eigenvalue analysis, where the presence of at least one eigenvalue with a positive real part indicates the fact that the open-loop linearized system is exponentially unstable.

3 LINEAR QUADRATIC REGULATOR DESIGN

3.1 Full-state feedback regulator

The bi-orthogonal basis generated by the Riesz-spectral operator $\mathfrak{A}$ in the LTI system $\Sigma(\mathfrak{A}, \mathfrak{B}, \mathfrak{C}, -)$ provides the foundation for solving the Operator Riccati Equation (ORE), a crucial step in the design of a Linear Quadratic Regulator (LQR). The objective is to determine an offline feedback control law that drives the system's states from an arbitrary initial condition to zero, thereby maintaining the system at its steady state. This is achieved within an optimal control framework, minimizing the infinite-time cost function defined in Equation 13. In this context, $\mathfrak{Q}$ and $\mathfrak{R}$ are self-adjoint coercive operators that penalize state deviations and control actions, respectively.

$$J(\boldsymbol{x_0}, u) = \int_{t=0}^{\infty} \langle \boldsymbol{x}(s), \mathfrak{Q}\boldsymbol{x}(s) \rangle + \langle u(s), \mathfrak{R}u(s) \rangle ds \tag{13}$$

3.1.1 Operator Riccati equation

The LQR problem is solved by finding the unique positive semi-definite operator $\boldsymbol{\Pi}$, which satisfies the ORE presented in Equation 14. This operator is then used to compute the feedback gain that ensures optimal control of the system.

$$\langle \mathfrak{A}^*\boldsymbol{\Pi}\boldsymbol{x}, \boldsymbol{y} \rangle + \langle \boldsymbol{\Pi}\mathfrak{A}\boldsymbol{x}, \boldsymbol{y} \rangle - \langle \boldsymbol{\Pi}\mathfrak{B}\mathfrak{R}^{-1}\mathfrak{B}^*\boldsymbol{\Pi}\boldsymbol{x}, \boldsymbol{y} \rangle + \langle \mathfrak{Q}\boldsymbol{x}, \boldsymbol{y} \rangle = 0 \tag{14}$$

Given that the solution to the ORE is unique for any set of functions in the domain of operator $\mathfrak{A}$, we can arbitrarily set $\boldsymbol{x} = \boldsymbol{\phi_m}$ and $\boldsymbol{y} = \boldsymbol{\phi_n}$, i.e. the eigenfunctions of $\mathfrak{A}$. Applying this choice, and noting that $\boldsymbol{\Pi}$ is self-adjoint, leads to the simplified Equation 15.

$$\langle \boldsymbol{\Pi}\boldsymbol{\phi_m}, \mathfrak{A}\boldsymbol{\phi_n} \rangle + \langle \mathfrak{A}\boldsymbol{\phi_m}, \boldsymbol{\Pi}\boldsymbol{\phi_n} \rangle - \mathfrak{R}^{-1}\langle \mathfrak{B}^*\boldsymbol{\Pi}\boldsymbol{\phi_m}, \mathfrak{B}^*\boldsymbol{\Pi}\boldsymbol{\phi_n} \rangle + \langle \mathfrak{Q}\boldsymbol{\phi_m}, \boldsymbol{\phi_n} \rangle = 0 \qquad (15)$$

To ensure that the domain and range of $\boldsymbol{\Pi}$ match those of $\mathfrak{A}$ and $\mathfrak{A}^*$, respectively, $\boldsymbol{\Pi}$ can be expressed as an infinite series, as shown in Equation 16. The coefficients $p_{i,j}$ can be interpreted as elements of an infinite-dimensional matrix $\tilde{P}$, which represents the operator $\boldsymbol{\Pi}$. This forms the first step in converting the ORE to the corresponding Matrix Riccati Equation (MRE).

$$\boldsymbol{\Pi}\boldsymbol{x} \equiv \sum_{i=1}^{\infty}\sum_{j=1}^{\infty} p_{i,j}\langle \boldsymbol{x}, \boldsymbol{\psi_j} \rangle \boldsymbol{\psi_i} \qquad \forall i, j: \quad p_{i,j} \in \mathbb{C} \qquad (16)$$

3.1.2 Obtaining $\mathfrak{B}$ and $\mathfrak{B}^*$

Before further simplifying the ORE, it is essential to define the operators $\mathfrak{B}$ and $\mathfrak{B}^*$. Given the boundary-control nature of the system as seen in Equation 3, $\mathfrak{B}$ is defined to properly project the control input $u \in \mathbb{R}^1$ onto the state space $X : L^2[0, 1] \times L^2[0, 1]$, as outlined in Equation 17.

$$\mathfrak{B}u \equiv v(1 - R)\begin{bmatrix} \delta(\zeta) \\ 0 \end{bmatrix} \cdot u \qquad (17)$$

where $\delta(\zeta)$ denotes the Dirac delta function. The adjoint operator $\mathfrak{B}^*$ is obtained by leveraging the properties of $\mathfrak{A}$ and $\mathfrak{A}^*$, i.e. their expressions as well as their domains (as shown in Equations 6 and 7), after applying integration by parts to the result of the inner products, as summarized in Equation 18.

$$\begin{aligned} \langle \mathfrak{A}\boldsymbol{x} + \mathfrak{B}u, \boldsymbol{y} \rangle &= \langle \mathfrak{A}\boldsymbol{x}, \boldsymbol{y} \rangle + \langle \mathfrak{B}u, \boldsymbol{y} \rangle = \langle \boldsymbol{x}, \mathfrak{A}^*\boldsymbol{y} \rangle + \langle u, \mathfrak{B}^*\boldsymbol{y} \rangle \\ \langle u, \mathfrak{B}^*\boldsymbol{y} \rangle &= \langle \mathfrak{A}\boldsymbol{x} + \mathfrak{B}u, \boldsymbol{y} \rangle - \langle \boldsymbol{x}, \mathfrak{A}^*\boldsymbol{y} \rangle \Rightarrow \ldots \\ &\Rightarrow \mathfrak{B}^*(\cdot) = \left[v(1 - R)\int_0^1 \delta(\zeta)(\cdot)d\zeta \quad , \quad 0 \right] \end{aligned} \qquad (18)$$

3.1.3 Matrix Riccati equation

Using the expression for $\boldsymbol{\Pi}$ in Equation 16, along with the derived $\mathfrak{B}^*$ from Equation 18, and the eigenvalue problem $\mathfrak{A}\boldsymbol{\phi_i} = \lambda_i\boldsymbol{\phi_i}$, the ORE can be reformulated as the Matrix Riccati

Equation (MRE) shown in Equation 19. Here, $\gamma_i \equiv v(1-R) \left. \psi_1^{(i)} \right|_{\zeta=0}$, and $q_{m,n} = \langle \mathfrak{Q}\phi_m, \phi_n \rangle$.

$$p_{n,m}(\lambda_m + \overline{\lambda_n}) - \mathfrak{R}^{-1}\langle \sum_{i=1}^{\infty} p_{i,m}\gamma_i, \sum_{i=1}^{\infty} p_{i,n}\gamma_i \rangle + q_{m,n} = 0 \tag{19}$$

Due to the infinite-dimensional nature of $\tilde{P}$, a numerical solution is impractical. This challenge is addressed by selecting the first N eigenmodes of the system as its dominant modes. This translates to truncating the infinite sums in the MRE and reducing the infinite-dimensional system to a finite set of nonlinear algebraic equations that can be solved to obtain an equivalent $N \times N$ matrix P, i.e. a truncated approximation of matrix $\tilde{P}$. The optimal full-state feedback gain is then calculated using Equation 20, ensuring closed-loop stability.

$$
\begin{aligned}
u(t) &= -\langle \boldsymbol{K}(\zeta), \boldsymbol{x}(\zeta,t) \rangle = -\mathfrak{B}^*\mathbf{\Pi}\boldsymbol{x}(\zeta,t) \\
&= -\sum_{i=1}^{N}\sum_{j=1}^{N} p_{i,j}\langle \boldsymbol{x}(\zeta,t), \boldsymbol{\psi_j}(\zeta) \rangle \gamma_i \\
&= -\sum_{i=1}^{N}\sum_{j=1}^{N} p_{i,j}\gamma_i \int_0^1 \boldsymbol{x}(\zeta,t) \cdot \overline{\boldsymbol{\psi_j}}(\zeta)d\zeta \\
&= -\int_0^1 \sum_{i=1}^{N}\sum_{j=1}^{N} p_{i,j}\gamma_i\overline{\boldsymbol{\psi_j}}(\zeta) \cdot \boldsymbol{x}(\zeta,t)d\zeta \\
\Rightarrow \boldsymbol{K}(\zeta) &\equiv \sum_{i=1}^{N}\sum_{j=1}^{N} p_{i,j}\gamma_i\overline{\boldsymbol{\psi_j}}(\zeta)
\end{aligned}
\tag{20}
$$

The computed gain is a function of space and is calculated offline. The control action at any given time instance is the inner product of this gain with the current state of the system, thus justifying the term "full-state" feedback. The dynamics of the resulting closed-loop full-state feedback system may be described by the state-space representation shown in Equation 21.

$$
\begin{aligned}
\dot{x}(\zeta,t) &= \mathfrak{A}\boldsymbol{x}(\zeta,t) + \mathfrak{B}u(t) \\
&= (\mathfrak{A} - \mathfrak{B}\boldsymbol{K})\,\boldsymbol{x}(\zeta,t) \\
&= \mathfrak{A}_{reg}\,\boldsymbol{x}(\zeta,t)
\end{aligned}
\tag{21}
$$

By selecting $\mathfrak{Q} = 0.05$ as a constant function over $\zeta = [0,1]$, and $\mathfrak{R} = 50$, the full-state feedback gain is obtained and represented in Figure 4. The obtained gains are used to design the optimal full-state feedback regulator to stabilize the control system. A block diagram representation of the full-state feedback control system is shown in Figure 5.
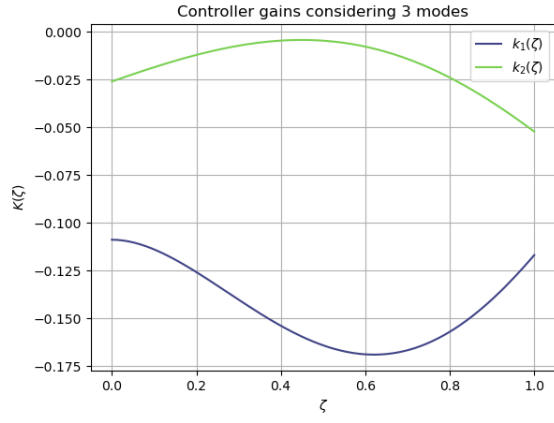
(A) $N = 3$
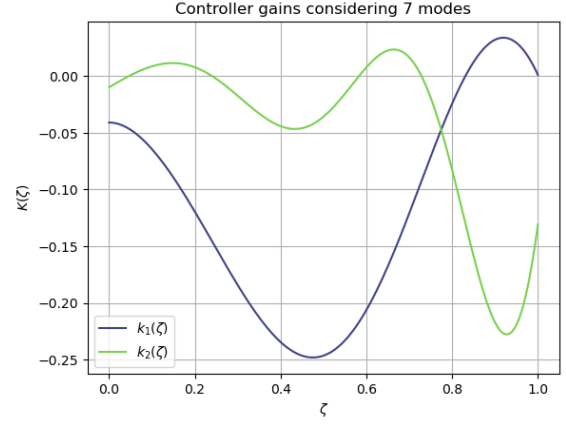
(B) $N = 7$

FIGURE 4: Full-state feedback gain $\boldsymbol{K}(\zeta)$ utilizing the first N modes of the system given by Equation (20).
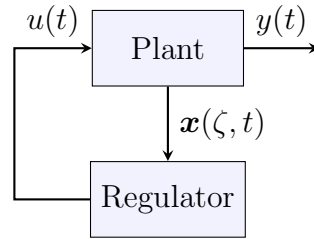

FIGURE 5: Block diagram representation of the optimal full-state feedback control system.

3.2 Output feedback compensator

Thus far, the optimal regulator is designed under the assumption that it has full access to the system's states. However, this assumption is not feasible in realistic applications. To address this, an observer is introduced to estimate and reconstruct the states by measuring the system's output in real time, and providing the regulator with the reconstructed states to further stabilize the system. The output, in this context, is taken as the concentration at the reactor outlet, as defined in Equation 3. This leads to the definition of the output operator $\mathfrak{C}$ in the linear time-invariant (LTI) system $\Sigma(\mathfrak{A}, \mathfrak{B}, \mathfrak{C}, -)$, which is subsequently used to determine the observer gain, $\boldsymbol{L}(\zeta)$. The formulation is shown in Equation 22:

$$\mathfrak{C} \equiv \left[\int_0^1 \delta(\zeta - 1)(\cdot)d\zeta \quad , \quad 0 \right] \tag{22}$$

where $\delta(\zeta)$ denotes the Dirac delta function. Regarding the choice of observer, Luenberger-based observers are well-suited for infinite-dimensional systems when the system parameters are perfectly known.[ali2015reviewobserver] Among the various methods to compute the gain for this class of observers, pole-placement is a solid, straightforward, and reliable approach for state reconstruction. To ensure that the state reconstruction dynamics converge more quickly than the regulation dynamics, the poles of the observer-based controller are placed to the left of the poles of the full-state feedback controller. This practice is common in the design of observer-based controllers for infinite-dimensional systems.[morrisbook] The observer gain in Figure 6 is obtained by limiting the eigenmodes of the observer-based controller to have real parts that are at least 3 times more negative than the real part of the dominant eigenmodes of the full-state feedback system. This is done for the case where the first 7 modes of the system are considered for designing the controller. The first few eigenvalues of the observer-based controller and the full-state feedback controller, along with the eigenvalues of the open-loop system are shown in Figure 7 to demonstrate the pole placement strategy explained above. It can be confirmed that both control systems have eigenvalues with negative real parts, ensuring stability. Note that the eigenvalues of both control systems are identical after the 7th mode, as the real parts of these eigenvalues are already sufficiently negative.

The dynamics of the augmented observer-controller system are described by the state-space representation shown in Equation 23, where $\hat{\boldsymbol{x}}(\zeta, t)$ and $\boldsymbol{e}(\zeta, t)$ refer to the estimated state and the state estimation error, respectively. A block diagram representation of the output feedback control system is also shown in Figure 8.
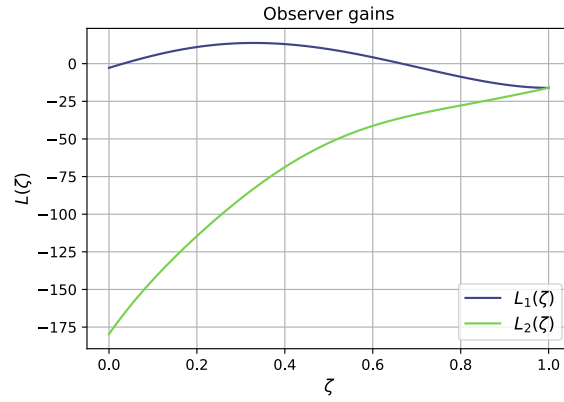
17

FIGURE 6: Observer gain $\boldsymbol{L}(\zeta)$.
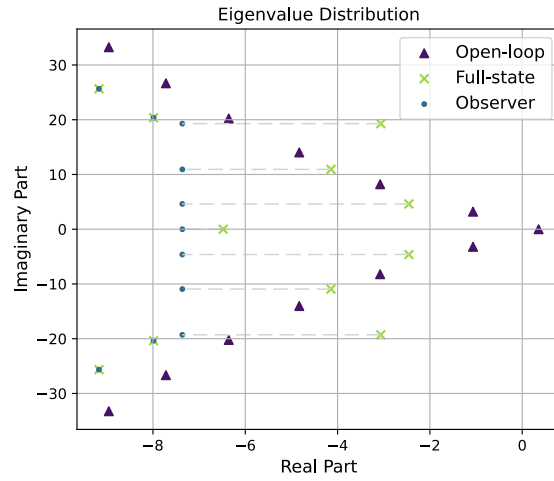

FIGURE 7: Eigenvalues of the observer-based controller, full-state feedback controller, and open-loop system.
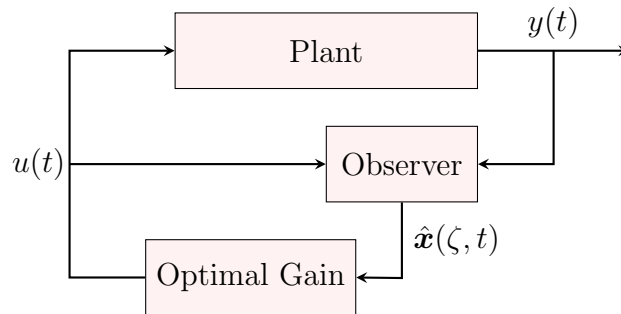

FIGURE 8: Block diagram representation of the observer-based output feedback control system.

$$\begin{bmatrix} \dot{\boldsymbol{x}}(\zeta,t) \\ \hline \dot{\hat{\boldsymbol{x}}}(\zeta,t) \end{bmatrix} = \begin{bmatrix} \mathfrak{A} & -\mathfrak{B}\boldsymbol{K} \\ \hline \boldsymbol{L}\mathfrak{C} & \mathfrak{A} - \mathfrak{B}\boldsymbol{K} - \boldsymbol{L}\mathfrak{C} \end{bmatrix} \begin{bmatrix} \boldsymbol{x}(\zeta,t) \\ \hline \hat{\boldsymbol{x}}(\zeta,t) \end{bmatrix}$$

$$\dot{\boldsymbol{e}}(\zeta,t) = \left[\dot{\boldsymbol{x}}(\zeta,t) - \dot{\hat{\boldsymbol{x}}}(\zeta,t) \right] \qquad (23)$$

$$= \left(\mathfrak{A} - \boldsymbol{L}\mathfrak{C} \right) \boldsymbol{e}(\zeta,t)$$

$$= \mathfrak{A}_{est}\, \boldsymbol{e}(\zeta,t)$$

4 RESULTS AND DISCUSSION

In this section, the obtained control strategies are applied to a finite-difference method (FDM) representation of the system to evaluate its dynamic response. The system is discretized in space using a uniform grid with 100 equidistributed points, resulting in a system of ordinary differential equations (ODEs) with respect to time. This spatial discretization is introduced solely at the evaluation stage to numerically approximate the system's behavior under the influence of the optimal control input and is not involved in the design of the control law. The control law is derived directly in the infinite-dimensional space, fully capturing the continuous nature of the original system.

To solve the resulting ODEs, an adaptive Runge-Kutta method of order 5(4), commonly referred to as RK45, is employed. This method dynamically adjusts time steps to balance accuracy and computational efficiency, ensuring a reliable numerical solution while evaluating the system at specific points as required.[RK45'1, RK45'2] The implementation of this method is facilitated using the `solve_ivp` function from Python's `SciPy` library,[2020SciPy] which provides a robust framework for handling time integration of ODEs.

Employing the outlined approach to evaluate the dynamic response of the systems under consideration, a comparative analysis is conducted between two identical systems with full-state access, differing only in the number of eigenmodes employed to compute the optimal full-state feedback gains. Subsequently, the performance of the proposed observer-based controller is assessed, with particular attention given to the dynamics of state reconstruction errors. Finally, a sensitivity analysis is performed to examine the impact of key parameters on the model behavior and the effectiveness of the control strategy. Across all simulations presented, $\mathfrak{Q} = 0.05 \cdot \mathfrak{I}$ and $\mathfrak{R} = 50$ are used as the deviation penalty and control effort weight operators, respectively, where $\mathfrak{I}$ denotes the identity operator matching the size of $\mathfrak{A}$.

## 4.1 Full-state feedback regulator FDM representation

Initially, the input response of the system provided by the full-state feedback is explored using the mentioned FDM setup. Two configurations are compared where the optimal feedback gain is obtained using different number of eigenmodes: one with $N = 3$ and another with $N = 7$, according to Figure 4. The state profile versus time and space is illustrated for both cases in Figure 9.
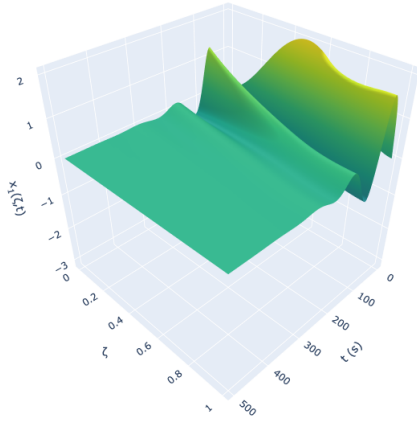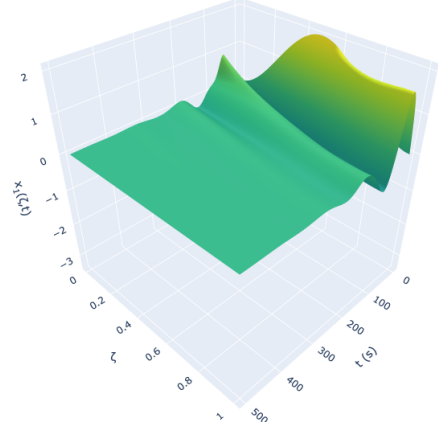
(A) $N = 3$ **(B)** $N = 7$

FIGURE 9: Input response of the system under full-state feedback control given by Equation (21), utilizing the feedback gain obtained in Figure 4.

    In order to offer a clearer representation of the state trajectory in time, spatial cross-sectional plots are provided in Figure 10 for the $N = 7$ case at different lengths of the domain. The delay-imposing state, i.e. the concentration along the recycle stream $x_2(\zeta, t)$, is provided only in Figure 10 for the sake of conciseness.

    Both optimal feedback gains are able to successfully stabilize the system within finite time horizon. However, the case where more eigenmodes are considered in the controller design shows better performance, as the higher dimensional controller is able to stabilize the system quicker with lower cost function values in general.
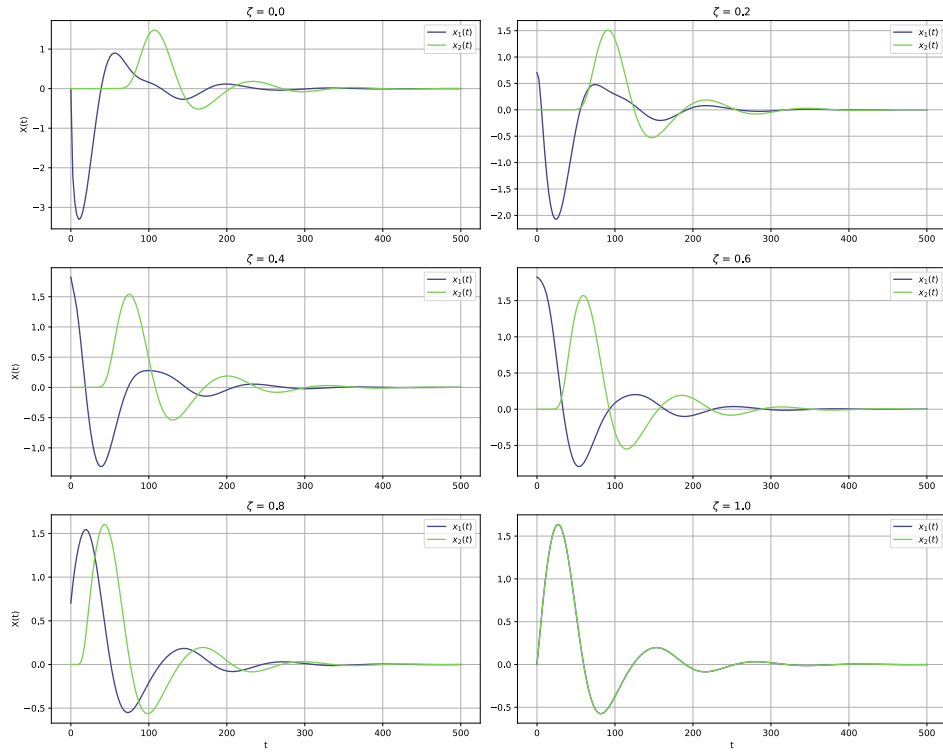
FIGURE 10: 2D cross-section plots of the full-state feedback input response at various ζ positions, utilizing the feedback gain obtained in Figure 4B.

4.2 Observer-based regulator FDM representation

Omitting the need to have full access to system states, the observer-based regulator is evaluated using the same FDM representation. The states reconstruction is done by applying the observer gain obtained in Figure 6 to the system output. The estimated states are now used with the previously obtained optimal feedback gain with $N = 7$ eigenmodes to calculate the input. Similar to the previous case, the state profile $x_1(\zeta, t)$ is illustrated in Figure 11, as well as cross-sectional plots for both states in Figure 12 for better visualization of state trajectories in time.
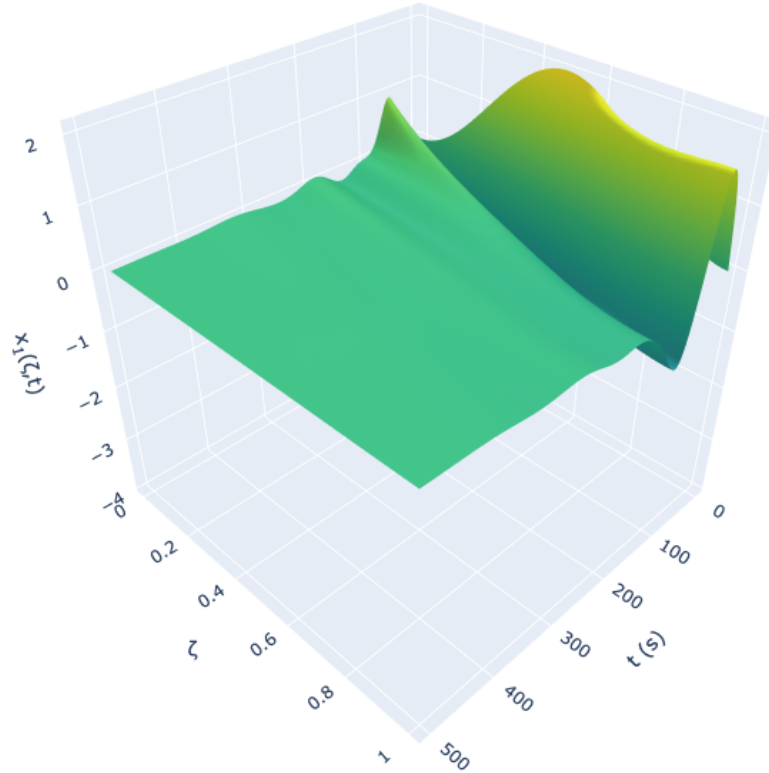

FIGURE 11: Input response of the system under observer-based output feedback control given by Equation (23), utilizing the observer gain obtained in Figure 6 and the feedback gain obtained in Figure 4B.
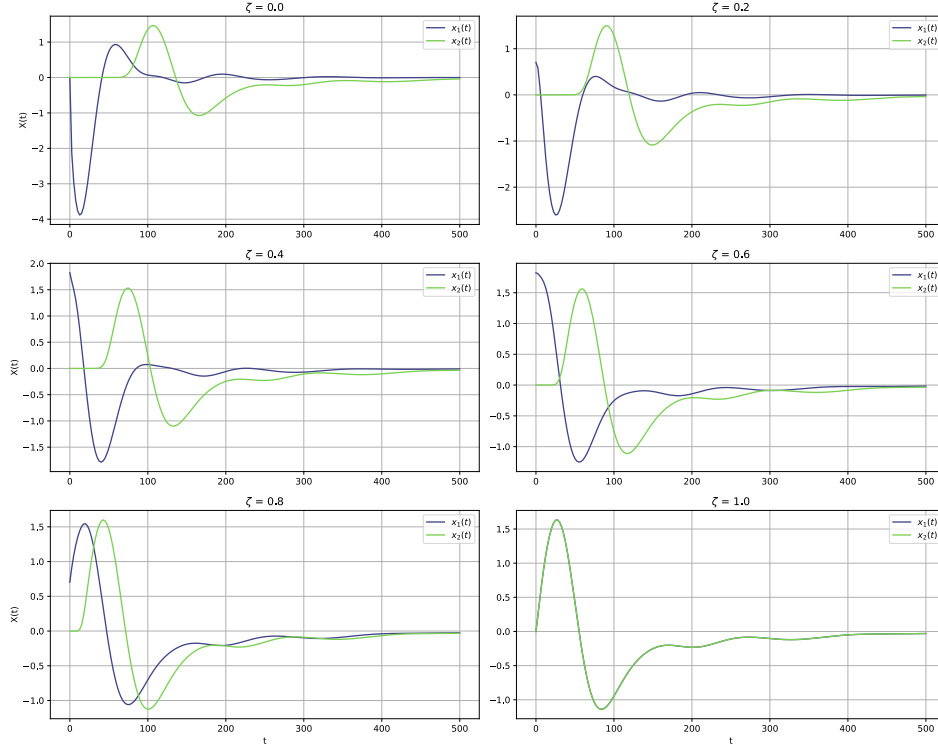
FIGURE 12: 2D cross-section plots of the input response at various ζ positions, utilizing the observer gain obtained in Figure 6 and the feedback gain obtained in Figure 4B.

In the next step, the state estimation error dynamics of the observer are plotted in Figures 13 and 14 to demonstrate the performance of the observer. The error dynamics are calculated as the squared difference between the true state and the estimated state at each grid point and time instance.

While the performance of the observer-based controller is slightly more sluggish compared to that of the full-state feedback regulator, it successfully stabilizes the system within a finite time horizon using only output measurements instead of full state information. In the absence of uncertainty in the system model, the observer gain can theoretically be designed so that the state estimation error converges to zero very fast compared to full-state feedback regulator dynamics. In practice, however, the observer gain is constrained by factors such as noise in the system output and plant-model mismatches. Despite these challenges, the proposed observer design mechanism achieves system stabilization with reasonable performance.

4.3 Parameter sensitivity analysis

Followed by showcasing the ability of the proposed controller to stabilize an unstable system using merely output measurements, a brief parameter sensitivity analysis of the model
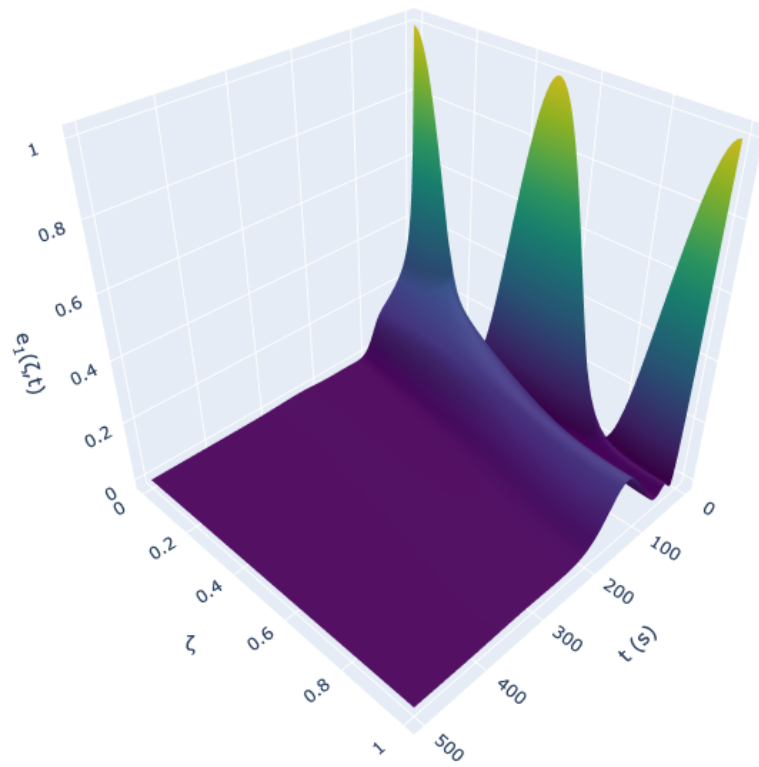
23

State reconstruction error profile

FIGURE 13: Error dynamics of the observer-based regulator utilizing the observer gain obtained in Figure 6 and the feedback gain obtained in Figure 4B.
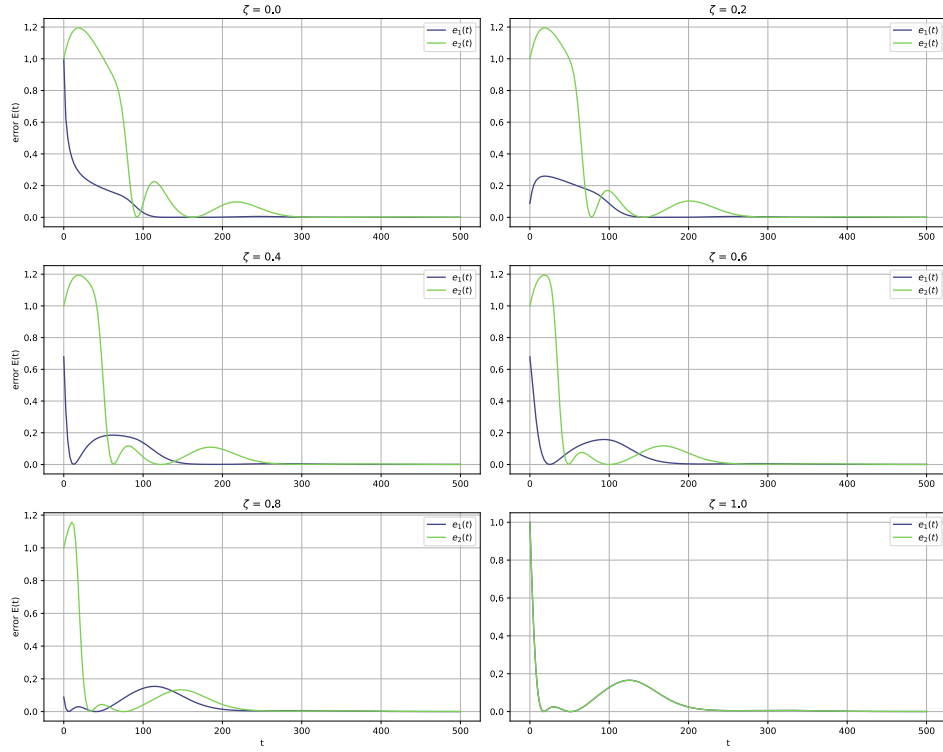
FIGURE 14: 2D cross-section plots of the error dynamics of the observer-based regulator at various ζ positions, utilizing the observer gain obtained in Figure 6 and the feedback gain obtained in Figure 4B.

dynamics and controller performance is conducted at the end of this section. The effects of varying the recycle ratio R and mass transfer Peclet number (i.e. the ratio of convection to diffusion, $Pe = v/D$) were explored during initial simulations. In addition, as it is central to this work, the effect of varying time delay τ on the response of the system under the original controller design is investigated in more detail.

Regarding the effect of recycle ratio on system dynamics and controller performance, it was observed that as the recycle ratio approaches unity, the open-loop system exhibits behavior similar to that of a well-mixed reactor, with concentration profiles flattening. This also influences the controller performance as it becomes more challenging to affect the system dynamics with the control input as the controller's action becomes diluted at the reactor inlet due to mixing with the recycle stream. For changes in mass Peclet number and its effect on the system dynamics, it was observed that a decrease in the Peclet number causes the eigenvalues of the system generator to shift closer to the real axis of the complex plane. This implies that greater diffusion relative to convection dampens the oscillatory behavior of the system that is originally imposed as the result of the delayed recycle stream.

Finally, the effect of varying time delay τ on the system dynamics is also investigated, as it is a key parameter in the model and controller design within this work. Input responses of several systems with different time delays are compared in Figure 15, where the input for all cases is calculated assuming $\tau = 80$ s, which results in the same output feedback gain as the one obtained in **Section 4.2**.

It can be seen that as long as the actual time delay of a system is less than the assumed delay used in the controller design, the controller is still able to stabilize the system within a finite time horizon, although transient deviations from the desired behavior are observed. However, as the actual delay increases, the response of the system starts to deviate significantly from the desired behavior, especially after a certain threshold close to the actual recycle delay of the system. This shows the importance of including the time delay in the controller design to ensure the stability of the system within an optimal framework.

Although further parameter sensitivity analysis is possible as it naturally raises readers' curiosity, expanding the analysis to include more detailed investigations would risk exceeding the scope of this work, which is to offer a novel modeling and control framework for a certain class of distributed parameter systems in chemical engineering. Nonetheless, the proposed modeling and control strategy is able to effectively stabilize the system over a broad range of parameter sets, including but not limited to variations in the imposed time delay, Peclet number, and recycle ratio, ensuring the practicality of the proposed framework across different system configurations.
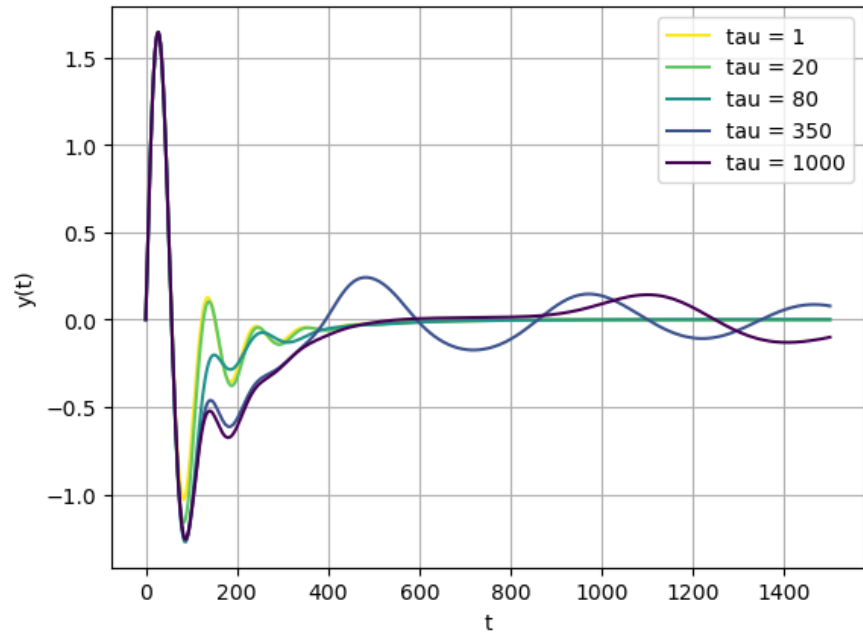
FIGURE 15: Measured output of the systems with different time delays τ, under observer-based output feedback control utilizing the observer gain obtained in Figure 6 and the feedback gain obtained in Figure 4B, where $\tau = 80$ s.

5 CONCLUSION

The control of an axial tubular reactor equipped with recycle stream is addressed as a significant class of distributed parameter systems in chemical engineering industries. The notion of time delay introduced by the recycle process has not been adequately addressed in the literature despite being a common and intrinsic feature of such systems; introducing a rare example of state-delay in this field. By converting the notion of delay into an equivalent transport PDE, the DPS is formulated as a system of coupled parabolic and hyperbolic PDEs. The infinite-dimensional system is assumed to be boundary controlled, with the control input acting on the reactor inlet. Particularly suited for the class of axial tubular reactors, Danckwerts boundary conditions are considered. A continuous-time linear quadratic optimal regulator is then developed to stabilize the system.

To address the infinite-dimensional nature of the system, a late lumping approach is employed, ensuring that the infinite-dimensional characteristics of the system are preserved in the control design. The system's Riesz-spectral properties are utilized to derive the full-state feedback regulator by solving the Operator Riccati Equation (ORE), utilizing dominant modes of the system to obtain low-dimensional feedback gains. Recognizing practical limitations of the full-state feedback strategy, an observer-based regulator is also introduced to reconstruct the system states using boundary measurements, addressing the challenge of limited state access in real-world applications.

The proposed framework may be extended to more complex diffusion-convection reactor configurations, such as non-isothermal reactors. More complex control strategies may also be considered for this framework, such as Model-Predictive Control (MPC) strategy, enabling constraints to be incorporated into the control design. The proposed observer-based control strategy may also be extended to handle measurement noise as well as plant-model mismatches, which are common in real-world applications. Another interesting aspect to explore is the briefly described impact that picking different numbers of eigenmodes may have on the optimality of controller design. This could be further investigated to provide a more comprehensive understanding of the effects of this choice on the controller's performance.

In summary, this research introduces a comprehensive optimal control strategy for a novel yet practically significant class of distributed parameter systems, i.e. axial tubular reactors with delayed recycle streams. A late-lumping approach is employed to address the infinite-dimensional nature of the system, leveraging the Riesz-spectral properties of the system generator to derive an optimal feedback law utilizing both full-state and estimated states of the system, setting the stage for future advancements in this area of research.

Nomenclature

Table 2: Nomenclature

Symbol	Description
k_r	Linearized reaction coefficient
t	Temporal coordinate
v	Flow velocity along the reactor
D	Diffusion coefficient
R	Recycle ratio
λ_i	Eigenvalue associated with eigenfunction ϕ_i
$\overline{\lambda_i}$	Complex conjugate of λ_i; Eigenvalue associated with adjoint eigenfunction ψ_i
τ	Residence time of the recycle stream
ζ	Spatial coordinate along the reactor (dimensionless, $0 \leq \zeta \leq 1$)
$c(\zeta, t)$	Concentration deviation from steady state along the reactor
$u(t)$	Control input applied at the reactor inlet
$\boldsymbol{x}(\zeta, t)$	State vector describing the system (e.g., concentration deviation and recycle states)
$y(t)$	System output measured at the reactor outlet
$C(\zeta, t)$	Concentration of the reactant A along the reactor
$\boldsymbol{K}(\zeta)$	Full-state feedback gain of the optimal controller
$\boldsymbol{L}(\zeta)$	Observer gain for the output feedback controller
$\boldsymbol{\phi}(\zeta)$	Eigenfunction of operator $\mathfrak{A}$
$\boldsymbol{\psi}(\zeta)$	Eigenfunction of adjoint operator $\mathfrak{A}^*$
$\mathfrak{A}$	State operator (system generator in state-space representation)
$\mathfrak{A}^*$	Adjoint state operator
$\mathfrak{B}$	Input operator (maps control input to state dynamics)
$\mathfrak{B}^*$	Adjoint input operator (maps state dynamics to control input)
$\mathfrak{C}$	Output operator (maps state dynamics to system output)
P	Truncated solution to the Matrix Riccati Equation (MRE)
$\mathfrak{Q}$	State penalty operator in the cost function
$\mathfrak{R}$	Control effort penalty operator in the cost function
Π	Solution to the Operator Riccati Equation (ORE)

Acknowledgements

Contributor Roles Taxonomy (CRediT) statement

Behrad Moadeli: Conceptualization, Methodology, Software, Formal analysis, Visualization, Writing - original draft, Writing - review & editing.

Guilherme Ozorio Cassol: Conceptualization, Methodology.

Stevan Dubljevic: Supervision, Funding acquisition, Project administration, Writing - review & editing.